JAN 31 1979

Item 830-A-15

NAS 1.60: 1398

NASA Technical Paper 1398

A Simplified Method for Calculating the Atmospheric Heating Rate by Absorption of Solar Radiation in the Stratosphere and Mesosphere

COMPLETED
ORIGINAL

Tatsuo Shimazaki and Leland C. Helmle

JANUARY 1979

NASA

(34)

NASA Technical Paper 1398

A Simplified Method for Calculating the Atmospheric Heating Rate by Absorption of Solar Radiation in the Stratosphere and Mesosphere

Tatsuo Shimazaki
Ames Research Center
Moffett Field, California
and
Leland C. Helmle
Informatics, Inc.
Palo Alto, California

National Aeronautics
and Space Administration

**Scientific and Technical
Information Office**

1979

A SIMPLIFIED METHOD FOR CALCULATING THE ATMOSPHERIC HEATING RATE BY ABSORPTION OF SOLAR RADIATION IN THE STRATOSPHERE AND MESOSPHERE

Tatsuo Shimazaki and Leland C. Helmle*

Ames Research Center

SUMMARY

A simple analytical formula is worked out for calculations of the atmospheric heating rate by absorption of solar radiation by O_3, H_2O, and CO_2. The method needs only seven parameters for each molecule and can save computational time and memory locations. It is particularly useful for heating calculations in three-dimensional global circulation models below 80 km. Applying the formula to the observed distributions of O_3, H_2O, and CO_2 produces reasonable latitudinal and seasonal variations in the heating rate. The calculated heating rate, however, is sensitive to the global distributions of the absorbing gases, and uncertainties in the O_3 distribution above ~50 km and the H_2O distribution below ~20 km may seriously affect the global distributions of the heating rate in these regions.

INTRODUCTION

Heating the atmosphere by solar radiation of wavelengths shorter than ~4 μ is the ultimate source of energy to drive the atmospheric motion. About 99% of the solar radiation energy is in this spectrum range with the maximum radiation at ~4828 Å corresponding to the 6000 K black body radiation. The main radiative processes in the earth's atmosphere for this spectrum range are absorption, reflection, and scattering; emission is entirely negligible because the atmospheric temperature is too low.

Calculations of the atmospheric heating rate due to gaseous absorption of solar radiation are essential in studies of radiative balance and global circulation models of the atmosphere. The main absorbing molecules are water vapor (H_2O) in the troposphere and ozone (O_3) in the stratosphere and mesosphere, whereas carbon dioxide (CO_2) is of secondary importance as an absorber throughout the region from troposphere to mesosphere. Molecular oxygen (O_2) becomes the dominant absorber in the thermosphere. The absorption of each constituent is highly selective and strongly dependent on wavelength, and calculations of the heating rate taking into account the detailed wavelength dependence are very time consuming if not impossible. To avoid such inconveniences and to facilitate the heating rate calculations, empirical formulae

*Informatics, Inc., Palo Alto, California 94303

have been developed by various investigators. Formulae differ widely, however, and in most cases different formulae have been used for different constituents and for different wavelength ranges even by the same author(s). Thus, we need different computer programs for calculating the heating rate in each case.

The purposes of this technical paper are (1) to calculate the heating rate due to O_3 absorption with high precision and to formulate this result and experimental results of heating due to H_2O and CO_2 absorption by Howard et al. (refs. 1 and 2) into a simple analytical expression; (2) to survey the existing formulae for heating rate calculations and compare our result with the results calculated by these formulae; and (3) to illustrate the global distribution of the heating rate calculated by our formula using the global data on O_3, H_2O, and CO_2 density distributions. Development of such an analytical formula is useful for simplifying the radiation calculations in global circulation models, since the computation time and storage locations are very limited by the fact that a large amount must be reserved for calculations of dynamics.

We intend to use the same formula used in calculations of the photodissociation rates of molecules at the Schumann-Runge band (Shimazaki et al., ref. 3), so that the heating rate and the photodissociation rate can be calculated by the identical formula. We need only several parameters in each calculation, and the same short subroutine can be used for calculations of both the heating rate and the photodissociation rate, thereby saving both computation time and storage locations.

METHOD OF ANALYSES

Heating by Ozone

Ozone absorbs solar radiation energy mainly at the Hartley band (2400 to 3000 Å), Huggins band (3000 to 3600 Å) and Chappuis band (4000 to 8500 Å). The division at 3000 Å between the Hartley and Huggins bands is somewhat arbitrary, and the Hartley band includes the wavelengths shorter than 2400 Å. The absorption by O_2 becomes increasingly important below 2400 Å, but heating by those absorptions should be small in the atmospheric region under our present concern. Since the absorption cross sections of ozone are well determined for the entire spectrum range, the exact heating rate can be calculated straightforwardly by

$$Q(\lambda,u) = I(\lambda)\sigma(\lambda)e^{-\sigma(\lambda)u} \tag{1}$$

where λ is the wavelength, u the total amount of ozone in cm atm NTP, I the incident solar energy flux, and σ the absorption cross section. I is related to the photon flux ϕ by the relation

$$I(\lambda) = \frac{hc}{\lambda}\phi \tag{2}$$

where h is the Planck's constant and c the speed of light. In the region of interest (below 80 km), the $O(^3P)$ formed by the ozone photolysis quickly recombines; the portion of energy spent for dissociation will be regained for atmospheric heating through chemical recombination processes. Thus, the energy loss by dissociation can be neglected.

The absorbed energy flux along the path is then calculated by

$$S(\lambda,u) = \int_o^u Q(\lambda,u)du = I(\lambda)[1 - e^{-\sigma(\lambda)u}] \tag{3}$$

In calculating equation (3) we used data for the solar flux from Detwiler et al. (ref. 4) and Ackerman (ref. 5) for the 2400 to 3000 Å range and from Thekaekara and Drummond (ref. 6) for the 3000 to 8500 Å range, and the data for the absorption cross section from Inn and Tanaka (ref. 7). The entire spectrum range 2400 to 8500 Å is divided into 122 subdivisions with the equal interval (50 Å), and the integrated solar flux and the averaged cross section have been calculated for each subdivision.

Taking the summation of equation (3) for the pertinent spectrum range would give the absorbed energy at the respective band

$$S(u) = \sum_{\lambda} S(\lambda,u) \tag{4}$$

The calculated absorbed energy is shown in figure 1 for the Hartley band, Huggins band, and Chappuis band, as well as for the total of the three bands. The abscissa indicates the ozone column density measured in cm atm NTP, and the corresponding scale for the height (km) is shown at the top for the three representative seasons and latitudes. In calculating these height scales, the diurnally averaged mass factor is multiplied by the vertical column density to obtain the total ozone density in the column along the oblique path in each case. Effects of the dependence of absorption on pressure are also incorporated for evaluating these height scales (see the later discussion on the effective mass for the pressure dependence of absorption).

It is seen in figure 1 that the solar energy is absorbed mainly at the Hartley band for u less than ~0.1 cm, whereas the absorption occurs mainly at the Chappuis band for u greater than ~1 cm. In the transition region there is a depression for the total of the three bands. The result of the calculations shown in figure 1 is fitted to the analytical expression

$$\log S = C_0 + C_1 \log u + C_2(\log u)^2 + \ldots + C_k(\log u)^k \tag{5}$$

for the range of u between 10^{-7} and 10^2 cm. The coefficients C_i are determined by the least square method so that the variations of the curves are best fitted with the equation (5). The resultant coefficients are tabulated in table 1(a) for the case of $k = 7$; for the total of three bands the result calculated from equation (5) is shown in figure 1 by a dash-dotted curve, which agrees well with the original solid curve. For the convenience

of some modelers, coefficients determined for the MKS system of units are given in table 1(b). The mean error of log S, or the mean relative error of S, is defined by

$$E(k) = \sqrt{\sum_{i=1}^{n} (\log S_4 - \log S_5)^2/(n - k)} \qquad (6)$$

where S_4 and S_5 are the values of S calculated by equations (4) and (5), respectively, n is the total number of observational points and k is the degree of the polynomial.

If the solar flux changes or is measured more accurately in the future, our method requires simply to modify C_0 to

$$C_0' = C_0 + \log I' - \log I \qquad (7)$$

where I and I' are the old and new solar flux, respectively, whereas all other coefficients C_i ($i \neq 0$) remain unchanged. The correction can also be made, if necessary, for the effects of changes in the sun-earth distance; the earth is about 3.28 percent closer to the sun in early January than in early July. The same method can also be used to calculate atmospheric heating by diffuse radiation reflected or scattered from clouds or ground. Using a known (or assumed) albedo, I' is then calculated from the downward radiation flux arriving at the reflection heights. The angular integration for the diffuse radiation is taken into account by using an air mass factor of 1.66. Using the more recent value 1.9 by Lacis and Hansen (ref. 8) would increase the calculated heating rate by diffuse radiation by ~5 percent.

Our result is compared with the results calculated by different formulae developed by other investigators in figure 2. Since the results are so close, the illustration of comparison of each model with our result is shown by shifting vertically with each other.

Manabe and Strickler (ref. 9) have used an analytical equation for absorptivity; multiplying the total incident solar energy (~2 cal cm^{-2} min^{-1} or ~1.39×10^6 erg cm^{-2} sec-1) to the absorptivity would give the total absorbed energy. As is seen in figure 2 their result is in good agreement with the present study for the range of u between 10^{-1} and 1 cm, which covers the main part of the stratosphere but gives much smaller absorption at larger values of u ($\geq$2 cm) and at smaller values of u ($\leq 10^{-3}$ cm). Thus their equation would cause serious errors and should not be used for the region above ~50 to 70 km (the actual height depends upon seasons and latitudes), where the path of the solar beam is smaller than ~10^{-3} cm, and for the region below ~25 km in winter at high latitudes, where the beam path is greater than ~2 cm.

Lacis and Hansen (ref. 8) used analytical formulae for absorptivities representing the spectrum of ultraviolet and visible radiation. As seen in figure 2, the total absorbed energy calculated for the two spectrum ranges

by their formulae is slightly smaller than the corresponding value calculated by our formula in most of the range of u except for the range between about 1 and 10 cm.

Lindzen and Will (ref. 10) have formulated the differential heating rate for the three bands into three different formulae. The absorbed energy can be calculated by integrating these equations from 0 to u. Using equations similar to those of Lindzen and Will, Strobel (ref. 11) has determined the new coefficients to calculate the heating rate for the three bands. The total absorbed energy calculated by these equations is compared with our result (fig. 2). Both Strobel and Lindzen formulae give absorbed energies in good agreement with the result of the present study for the range of u between 10^{-2} and 10 cm, which covers most regions of the stratosphere. Our formula gives, however, generally larger absorption than most other formulae, and part of the reason for this difference may be caused by the fact that our analyses include wider spectra, although the ranges are not always clearly stated in some models.

Heating by Water Vapor

Water vapor is the main absorber of solar radiation in the troposphere. Howard et al. (ref. 2) have formulated their experimental results for integrated absorption function for seven bands (6.3 μ, 3.2 μ, 2.7 μ, 1.87 μ, 1.38 μ, 1.1 μ, and 0.94 u) into the following formulae

$$\int_{\Delta\nu} A_\nu d\nu = cu^d(p + e)^k \tag{8}$$

for weaker absorption, and

$$\int_{\Delta\nu} A_\nu d\nu = C + D \log u + K \log (p + e) \tag{9}$$

for stronger absorption, where u is the water vapor column density in g cm^{-2}, p and e represent the total pressure and the partial pressure of water vapor in mm Hg, respectively. The constants c, d, k, C, D and K are given for each band (see Burch et al., ref. 12, for the revised values for these constants). The absorbed solar energies calculated using these equations are shown for each band and for the total of seven bands in figure 3. Sudden jumps on some curves are caused by the transition between the range where the weaker absorption form (8) is applicable and the range where the stronger absorption form (9) is applicable. There is no apparent discontinuity on the curve for the total of seven bands. We have fitted the total curve with equation (5) for the range of u between 10^{-7} and 10^{2} g cm^{-2}; the determined coefficients for the seventh-order polynomial are tabulated in table 2. The variation calculated by this equation agrees well with the original variation which is shown by a dot-dashed curve in figure 3.

Many attempts have been made in the literature to express the solar energy absorbed by water vapor in simple analytical forms, and the results

of calculations by these formulae are compared in figure 4. The formula of Mügge and Möller (ref. 13) is essentially the first-order polynomial of the type of equation (5), and changing the units from cal cm^{-2} min^{-1} to erg cm^{-2} sec^{-1}, their equation can be written as

$$\log S = 5.079 + 0.303 \log mu \tag{10a}$$

where m is the air mass factor. Our corresponding equation is expressed as

$$\log S = 5.007 + 0.429 \log mu \tag{10b}$$

Korb et al. (ref. 14) have improved equation (10a) and obtained the third-order polynomial

$$\log S = 5.1036 + 0.347 \log mu - 0.056 (\log mu)^2 - 0.006 (\log mu)^3 \tag{11a}$$

which can be compared with our third-order polynomial

$$\log S = 5.0791 + 0.3150 \log mu - 0.0416 (\log mu)^2 - 0.0029 (\log mu)^3 \tag{11b}$$

The result from the Korb formula gives the closest variation to the present result, which is very close to the one calculated from the formula of Howard et al. As seen from table 3, the mean error of our third-order polynomial is about 2.4 times larger than the mean error of the seventh-order polynomial; therefore, it is preferable to use the seventh-order polynomial.

The analytical forms of Sasamori et al. (ref. 15) and Lacis and Hansen (ref. 8) are both based on absorptivities evaluated with the radiation chart of Yamamoto (ref. 16); thus, the general tendency of the variation in these two results is similar over the range of mu = 10^{-2} - 10 cm for which the formulae may have been approximated. Extension of the formulae beyond this range causes large discrepancies between the two results. It is seen in figure 4 that the formula of Howard et al. (ref. 2) gives smaller absorption than most other formulae for the range of u greater than ~10^{-2} g cm^{-2}, whereas it gives larger absorption for the smaller u than this value.

Heating by Carbon Dioxide

Howard et al. (ref. 1) have used the same formulae as equations (8) and (9) to express their experimental data on the absorption by CO_2 in eight bands (14.7 μ, 5.2 μ, 4.8 μ, 4.3 μ, 2.7 μ, 2.0 μ, 1.6 μ, and 1.4 μ). The calculated absorption in each band and the total of eight bands are shown in figure 5. The large jump appearing in the curve of the 4.3 μ band causes a discontinuity for the curve of total of eight bands, since the 4.3 μ band gives the largest contribution. We have smoothed in the region of the discontinuity and have then applied the curve fitting process using equation (5) for the range of u between 10^{-7} and 10^3 cm. The coefficients determined for the seventh-order polynomial are tabulated in table 2 along with the mean errors in each case of third to seventh-order polynomials.

DISTRIBUTION OF GASES

To calculate the atmospheric heating rate using the analytical formula developed in previous sections, we need the data of global distributions of absorbing gases.

Ozone

The general latitudinal and seasonal variations of the vertical ozone distributions up to ~35 km are reasonably well known. We have used data analyzed and compiled by Wilcox et al. (ref. 17) based on ozonesonde data obtained at various stations in the world from 1957 to 1972. Wilcox et al. give the ozone densities for every 2.5 km up to the height of 32.5 km, and we have interpolated these values to obtain the ozone densities at every km interval. For the region above 30 km up to ~55 km, the satellite measurements of backscatter ultraviolet (BUV) solar radiation from the atmosphere can give the information of ozone profiles on a global basis. Taking the data at 50 km obtained by the Nimbus-4 satellite experiments (I. Eberstein, private communication, 1977) and combining it with the ozonesonde data at 32.5 km, we have calculated by interpolation and extrapolation the ozone densities at every km up to the height of 80 km, assuming the exponential decrease with height. The result is shown in figure 6(a) for March (northern spring and southern fall) and in figure 6(b) for June (northern summer and southern winter).

Water Vapor

The distribution of water vapor mixing ratio in the troposphere is expressed in the analytical form of

$$F_{H_2O} = f(z)e^{-sx} \tag{12}$$

where x is the latitude, z is the height and s is the parameter changing sinusoidally with season from 0.016 in summer to 0.032 in winter. These values of s and the functional form of $f(z)$ are determined based on data published by Oort and Rasmusson (ref. 18). The adopted values of $f(z)$ are given in table 3. In the stratosphere the mixing ratio is assumed to be constant at 3.5×10^{-6}. Since the tropopause is low (~8 km) at high latitudes, the above procedure would cause sudden large changes in the water vapor mixing ratio at ~8 km at latitudes above ~60°, as is seen in figures 7(a) and (b).

Carbon Dioxide

We assume the constant mixing ratio of 3.2×10^{-4} for CO_2. Recent model calculations (Shimazaki, unpublished result) indicate that the mixing ratio decreases slightly with height (from 3.2×10^{-4} at the ground to ~1.86×10^{-4} at 60 km), but this slight change should not greatly affect the calculation of

the atmospheric heating rate, since the CO_2 absorption is not the primary source of the atmospheric heating.

RESULT AND DISCUSSION

Calculating the absorbed energy in the atmosphere by equation (5), we have taken into account the dependence of absorption on pressure by introducing the effective mass of the radiative absorbent

$$u_{eff} = u\left(\frac{P}{P_o}\right)^n \tag{13}$$

where P_o is the normal pressure of one atmosphere (1013.25 mb). For H_2O and CO_2 the power n can be evaluated from k/d in equation (8) and from K/D in equation (9), and the average values for all bands under consideration give ~0.6 for H_2O and ~0.8 for CO_2. The power n for O_3 is taken as 0.2 referring to Kondratyev (ref. 19).

The global average of height profiles of the heating rate calculated for each constituent for March is illustrated in figure 8. The figure demonstrates the strong effect of n on the heating rate by O_3 absorption in regions above ~40 km. The value of 0.4 has been obtained for n by McClatchy et al. (ref. 20), but it is inappropriate to use this value for the ultraviolet range, since it would give too small heating rate above ~35 km as is seen in figure 8. McClatchy's value is based on the experimental data on ozone transmittance for the infrared radiation. The result for $n = 0$ gives too much heating above ~50 km particularly at high latitudes.

Heating by the reflected solar radiation is calculated assuming the global average of the effective albedo to be 0.25. The effective albedo takes into account the combined effect of reflection from clouds and the ground surface and is useful in calculating the heating by the reflected waves above the clouds. The present study is concerned mainly with the stratosphere and mesosphere, and the concept of the effective albedo should give the reasonable heating rate in these regions. It is essential, however, for the troposphere to take into account the cloud albedo and the surface albedo separately and to calculate the radiative heat fluxes between the cloud and the ground surface and also within the clouds.

The calculated heating rates by reflected waves due to H_2O and CO_2 absorption are very small in the stratosphere (fig. 8). Furthermore, since the albedo of clouds is relatively small in the infrared and also since water vapor droplets in clouds absorb radiation almost at the same spectrum as water vapor, the heating by reflected waves due to H_2O and CO_2 absorption should be smaller than those shown in figure 8 and can be entirely neglected. On the other hand, the albedo of clouds is high in the visible and ultraviolet, therefore heating by the reflected waves due to the O_3 absorption cannot be neglected. In fact, as is seen in figure 8, this heating is comparable to the heating by CO_2 (direct radiation) in the lower stratosphere, and is about 22 percent of the O_3 heating by direct radiation at 25 km.

Applicability of our formula is limited to the range of u greater than 10^{-7} g cm^{-2} for H_2O and 10^{-7} cm atm NTP for O_3 and CO_2; these critical values are met somewhere above ~40 km for H_2O and above ~80 km for CO_2 and O_3 (see the top abscissa of figs. 1, 3, and 5), although these heights depend upon the season and latitude and should be much higher near the sunrise and sunset times. The heating rate in the regions outside of these critical heights are not shown in figure 8 and are neglected in our calculation of atmospheric heating. Fortunately, however, contributions from these heatings are generally small and their neglect should not affect the global distribution of the total heating rate in the region below 80 km. The upper limits of the formula's applicability are 10^2 g cm^{-2} for H_2O, 10^2 cm atm NTP for O_3 and 10^3 cm atm NTP for CO_2. The column densities of the absorbents are usually within these limits.

The heating rate due to CO_2 and H_2O absorption represented in terms of °K per day is almost constant above certain heights (fig. 8). This phenomenon is caused by the assumption of the constant mixing ratio, that is, these constituents' concentrations change with height in proportion to the mass density of atmosphere. Since the heat capacity also decreases with height in proportion to the mass density of the atmosphere, the rate of change in temperature should remain almost constant with height, although the actual absorbed energy decreases with height.

Latitudinal distributions of the diurnal heating rate are illustrated in figures 9(a) and 9(b) for March and June, respectively, in terms of temperature change per day. The top 1 to 2 km region is affected by the assumption on the total amount of O_3 above the upper boundary: we assume that the O_3 density decreases above 80 km with the scale height of its own mass. The actual distribution is complicated and has some bulge around 80 km (see, for instance, Schimazaki and Laird, ref. 21). For March, the global maximum occurs around 40 to 45 km in the equatorial region. Whereas the distribution is almost symmetrical around the equator in regions below this height, a marked asymmetry appears in higher regions; the larger heating rate is calculated at high latitudes in the southern hemisphere. This is certainly related to the larger ozone density calculated in that same area (see fig. 6(a)).

It is well known that there is a worldwide maximum of the total ozone density at the northern high latitudes in March and April. This tendency is clearly seen in the ozone density at ~30 km in figure 6(a); that is, the ozone density observed at the northern high latitudes is appreciably larger than the corresponding values at the southern high latitudes. It is not certain, however, whether or not this tendency should remain the same in the higher regions since contribution of that region to the total ozone density is very small.

The ozone density above 50 km shown in figure 6(a) is calculated by extrapolation from the ozonesonde value at 32.5 km and the BUV value at 50 km. The larger ozone density above 50 km at the southern high latitudes results from the fact that the ozone density is relatively low at 32.5 km, whereas the value at 50 km is about the same between the southern and

northern high latitudes. There may be little hemispheric difference for ozone density in the entire region above 50 km, but the larger ozone density above 50 km calculated in the southern high latitudes is consistent with the smaller density in the lower region, since the larger ozone density at higher region should absorb more radiation, making the radiation available for ozone production smaller in the lower region. However, it is true that there is a great uncertainty on the latitudinal distribution of the ozone density (and therefore the heating rate) above 50 km.

Calculating the heating rate assuming the uniform distribution of ozone density with latitudes represented, for instance, by the distribution at 35° N, we obtain the uniform distribution of the heating rate with latitude above ~50 km. The distribution below this height is affected very little; the general features are similar to those shown in figure 9(a). It is evident that the global distribution of heating rate is sensitive to the ozone density distribution. Unfortunately, there is no direct measurement of global distribution above 50 km. Rocket observations provide scant data for limited locations and time period. Since the atmospheric scattering is very weak above ~55 km, there is a practical upper limit of the altitude from which ozone information may be obtained by the BUV method. A good theoretical model would be useful in filling this information gap.

Heating below ~20 km is mainly due to H_2O absorption, and the high density of H_2O near the surface in the lower latitudes shown in figure 7(a) causes an increase of the heating rate in that region.

For June there is a global maximum of the heating rate at ~50 km near the north (summer) pole (see fig. 9(b)). Above this height, we again see the effect of the nonuniform distribution of the ozone density shown in figure 7(b). Below ~20 km where the heating by H_2O is dominant, we see a large heating in the summer at high latitudes, particularly near the tropopause (~8 km). This is caused by the sudden change of the humidity from the troposphere to the stratosphere. Since the tropopause is relatively low at high latitudes, and since we have assumed the same small mixing ratio for H_2O for the entire stratosphere, the model has produced a very large sudden change of the H_2O concentration at the tropopause at high latitudes (see fig. 7(a) and (b)).

The horizontal distribution of the heating rate is shown in figure 10(a) through (h) at every 10 km for the month of June. At the surface, the maximum heating occurs at ~10° north of the equator (summer) around noon (180° of longitude) and decreases rather steadily in all directions. At 10 km, a slow variation occurs from the equator to ~55° N during the midday period, and a sudden decrease appears at the northern end. This is caused by the sudden change of H_2O concentration; the 10 km level is in the troposphere (wet atmosphere) at the lower latitudes, whereas it is in the stratosphere (dry atmosphere) at the higher latitudes.

Above 20 km, the ozone heating is the dominant heat source, and the single maximum appears in the distribution at 30 and 40 km. There are two maxima, however, one larger maximum at the northern summer high latitudes

(~50 to 70°) and a smaller maximum at the southern winter latitudes (~35 to 50°) at 20 and 50 to 70 km. The latitude where the maximum appears shifts towards higher latitudes as the altitude goes up. These features of the maximum heating rates directly reflect the similar features of the single and double maxima in the distribution of the ozone density (see fig. 6(b)).

CONCLUDING REMARKS

This study presents a convenient analytical formula for calculations of the atmospheric heating rate. Its form is identical to that used for calculations of the photodissociation rate at the O_2 Schumann-Runge band system (Shimazaki et al., ref. 3); it should be useful for reducing the computational time and memory allocation for computer programs in heating and dissociation calculations in three-dimensional global circulation models. We plan to work out similar formulation for dissociation calculations for many other molecules at different wavelength ranges.

The mean relative error of our formula for calculations of ozone heating is ~2.4 percent of the exact calculations, and our formulae for H_2O and CO_2 are within 1% of the calculations by formulae of Howard et al. (refs. 1 and 2). The formulae of Howard et al. can predict their observations to ±3%. The larger error for ozone heating calculations than for H_2O and CO_2 heating calculations is caused mainly by the fact that we calculate the heating rate due to the three bands by a single equation. These three bands are at very different wavelength ranges. Tables 1(a) and 1(b) include the coefficients that should be used for each band separately. Using such coefficients can reduce the mean error for ozone heating calculations; it would also be useful for some specific purpose, such as detailed calculations of the change in the heating rate at the ozone cut-off range near 3000 Å, when the ozone density changes largely from the currently observed value.

Our formula can be used only for the range of column density greater than 10^{-7} cm atm NTP for O_3 and CO_2, and 10^{-7} g cm^{-2} for H_2O. These values cover most regions below 80 km except for the H_2O heating above ~40 km. However, the heating by H_2O in this region should not affect the total heating rate. The ozone heating by the reflected solar short waves contributes about 20 to 30% of the heating by the direct solar radiation in regions of 20 to 30 km.

The calculated atmospheric heating rate and its global distribution are reasonable, but they are sensitive to the ozone density distribution in the stratosphere and the mesosphere and to the water vapor distribution below 20 km. The global ozone distribution above 50 km is not known well, and observational as well as theoretical studies for this region should be

important. The distribution of water vapor in the troposphere and its change through the tropopause are also important for calculating the realistic distribution of the heating rate below ~20 km.

Ames Research Center
National Aeronautics and Space Administration
Moffett Field, Calif. 94035, July 19, 1978

REFERENCES

1. Howard, J. N.; Burch, D. E.; and Williams, Dudley: Infrared Transmission of Synthetic Atmosphere. II. Absorption of Carbon Dixoide. J. Opt. Soc. of America, vol. 46, no. 4, April 1956, pp. 237-241.

2. Howard, J. N.; Burch, D. E.; and Williams, Dudley: Infrared Transmission of Synthetic Atmospheres. III. Absorption of Water Vapor. J. Opt. Soc. of America, vol. 46, no. 4, April 1956, pp. 242-245.

3. Shimazaki, Tatsuo; Ogawa, Toshihiro; and Farrell, B. C.: Simplified Methods for Calculating Photodissociation Rates of Various Molecules in Schumann-Runge Band Systems in the Upper Atmosphere. NASA TN D-8399, 1977, p. 39.

4. Detwiler, C. R.; Garrett, D. L.; Purcell, J. D.; and Tousey, R.: The Intensity Distribution in the Ultraviolet Solar Spectrum. Ann. Geophys., vol. 17, 1961, pp. 263-272.

5. Ackerman, M: Ultraviolet Solar Radiation Related to Mesospheric Processes. Mesospheric Models and Related Experiments. G. Fiocco, ed., D. Reidel, Dordrecht, Holland, 1971, pp. 149-159.

6. Thekaekara, M. P.; and Drummond, A. J.: Standard Values for the Solar Constant and Its Spectral Components. Nature, Phys. Sci., vol. 229, 1971, pp. 6-9.

7. Inn, Edward C.Y.; and Tanaka, Yoshio: Absorption Coefficient of Ozone in the Ultraviolet and Visible Regions. J. Opt. Soc. Amer., vol. 43, no. 10, Oct. 1953, pp. 870-873.

8. Lacis, Andrew A.; and Hansen, James E.: A Parameterization for the Absorption of Solar Radiation in the Earth's Atmosphere. J. Atmos. Sci., vol. 31, no. 1 Jan. 1974, pp. 118-133.

9. Manabe, Syukuro; and Strickler, Robert F.: Thermal Equilibrium of the Atmosphere with a Convective Adjustment. J. Atmos. Sci., vol. 21, no. 4, July 1964, pp. 361-385.

10. Lindzen, R. S.; and Will, D. I.: An Analytical Formula for Heating due to Ozone Absorption. NASA CR-132778, Aug. 1972, p. 8.

11. Strobel, Darrell F.: Parameterization of the Atmospheric Heating Rate from 15 to 120 km due to O_2 and O_3 Absorption of Solar Radiation. NRL Memorandum Report 3398, 1976, p. 26.

12. Burch, D. E.; Gryvnak, D.; Singleton, E. G.; France, W. L.; and Williams, D.: Infrared Absorption by Carbon Dioxide, Water Vapor, and Minor Atmospheric Constituents. Research report, AFCRL-62-698, 1962, p. 316.

13. Mügge, R.; and Möller, F.: Zur Berechnung von Strahlungsströmen und Temperaturänderungen in Atmosphären von beliebigem Aufbau. Z. fur Geophysik, vol. 8, 1932, pp. 53-64.

14. Korb, Günther; Michalowsky, Johannes; and Möller, Fritz: Investigations on the Heat Balance of the Troposphere. Air Force Cambridge Research Center, TN-58-238, 1957.

15. Sasamori, Takashi; London, Julius; and Hoyt, Douglas V.: Radiation Budget of the Southern Hemisphere. Meteorological Monographs, vol. 13, no. 55, Nov. 1972, pp. 9-23.

16. Yamamoto, Gi-ici: On a Radiation chart. Science Rept. Tohoku Univ. Japan, Series 5, Geophysics, vol. 4, no. 1, June 1952, pp. 9-23.

17. Wilcox, R. W.; Nastrom, G. D.; and Belmont, A. D.: Periodic Analysis of Total Ozone and Its Vertical Distribution. Control Data Corporation, NASA CR-137737, Aug. 1975, p.27.

18. Oort, A. H.; and Rasmusson, E. M.: Atmospheric Circulation Statistics, NOAA Professional Paper 5, U. S. Dept. Commerce, Sept. 1971, p. 323.

19. Kondratyev, K. Ya: Radiation in the Atmosphere. Academic Press, New York and London (translated from Russian), 1969, p. 912.

20. McClatchey, R. A.; Fenn, R. W.; Selby, J.E.A.; Volz, F. E.; and Garing, J. S.: Optical Properties of the Atmosphere. 3rd edition Air Force Cambridge Research Laboratory Environmental Research Paper No. 411, Aug. 1972, p. 108.

21. Shimazaki, Tatsuo; and Laird, A. R.: A Model Calculation of the Diurnal Variation in Minor Neutral Constituents in the Mesosphere and Lower Thermosphere Including Transport Effects. J. Geophy. Res., vol. 75, no. 16, June 1970, pp. 3221-3235.

TABLE 1(a).- COEFFICIENTS OF THE SEVENTH-ORDER POLYNOMIAL FOR HEATING CALCULATIONS DUE TO O_3 ABSORPTION AND MEAN RELATIVE ERROR FOR THIRD- TO SEVENTH-ORDER POLYNOMIALS (CGS UNITS)

Spectrum range	Hartley band, 2400-3000 Å	Huggins band, 3000-3600 Å	Chappuis band, 4000-8500 Å	Total, 2400-8500 Å
Incident solar energy (erg · cm^{-2} sec^{-1})				
I	1.406(4)[α]	5.915(4)	6.918(5)	8.097(5)
Coefficients				
C_0	4.14292071(0)	4.23361218(0)	4.43346790(0)	4.75812947(0)
C_1	-5.33910483(-2)	4.12314108(-1)	9.50434910(-1)	4.93805176(-1)
C_2	1.38771166(-2)	-1.60939373(-1)	-6.23836459(-2)	1.26465765(-1)
C_3	5.36079604(-2)	1.26356978(-2)	-3.20014961(-2)	2.10425653(-2)
C_4	-8.90746861(-3)	9.98975983(-3)	-7.37424271(-3)	-2.45982304(-2)
C_5	-6.07296255(-3)	6.52086922(-4)	-6.81798995(-4)	-7.96267282(-3)
C_6	-8.42668609(-4)	-1.25888537(-4)	-1.89154394(-6)	-8.71717239(-4)
C_7	-3.75005646(-5)	-1.27022887(-5)	2.17012054(-6)	-3.24914714(-5)
Mean relative errors				
E(3)	1.264(-1)	4.413(-2)	5.796(-2)	1.043(-1)
E(4)	5.294(-2)	4.429(-2)	2.708(-2)	6.865(-2)
E(5)	4.339(-2)	2.348(-2)	9.653(-3)	6.588(-2)
E(6)	2.365(-2)	1.361(-2)	5.576(-3)	2.795(-2)
E(7)	1.678(-2)	1.255(-2)	5.583(-3)	2.419(-2)

[α] A(b) should read as $A \times 10^b$.

TABLE 1(b).- COEFFICIENT OF THE SEVENTH-ORDER POLYNOMIAL FOR HEATING CALCULATIONS DUE TO O_3 ABSORPTION (MKS UNITS)

Spectrum range	Hartley band, 2400-3000 Å	Huggins band, 3000-3600 Å	Chappuis band, 4000-8500 Å	Total, 2400-8500 Å
Incident solar energy ($J \cdot m^{-2} \cdot sec^{-1}$)				
I	1.406(1)[α]	5.915(1)	6.918(2)	8.097(2)
Coefficients				
C_0	1.12492560(0)	1.68658866(0)	2.68914243(0)	2.71161737(0)
C_1	-3.04055682(-1)	2.62163034(-1)	2.69717248(-2)	-3.53904066(-1)
C_2	-5.91532217(-1)	1.68046817(-1)	-4.84914017(-1)	-1.20569660(0)
C_3	-4.16397584(-1)	9.13818058(-2)	-1.17354777(-1)	-6.51920173(-1)
C_4	-1.30697369(-1)	5.40067599(-3)	-1.36980916(-2)	-1.65625605(-1)
C_5	-1.93350333(-2)	-1.92556778(-3)	-5.22207398(-4)	-2.11525633(-2)
C_6	-1.36767651(-3)	-3.03720579(-4)	2.84901436(-5)	-1.32659784(-3)
C_7	-3.75005646(-5)	-1.27022887(-5)	2.17012054(-6)	-3.24914714(-5)

[α] A(b) should read as A × 10^b.

TABLE 2.- COEFFICIENTS OF THE SEVENTH-ORDER POLYNOMIAL FOR HEATING CALCULATIONS DUE TO H_2O AND CO_2 ABSORPTION AND MEAN RELATIVE ERROR FOR THE THIRD- TO SEVENTH-ORDER POLYNOMIALS

	CGS Units		MKS Units	
Spectrum range	H_2O	CO_2	H_2O	CO_2
Incident solar incident				
I	3.292(5)[α]	1.162(5)	3.292(2)	1.162(2)
Coefficients				
C_0	5.05447794(0)	3.53768885(0)	1.73903147(0)	1.10124356(0)
C_1	2.91792812(-1)	3.70827458(-1)	3.53646788(-1)	2.46467496(-1)
C_2	-8.46611844(-3)	-5.91767097(-2)	-5.04237590(-2)	1.95386476(-2)
C_3	1.37174940(-2)	9.35607274(-4)	8.61937376(-3)	2.20605560(-2)
C_4	-4.03685379(-3)	3.04430731(-3)	4.51071951(-3)	4.65717546(-4)
C_5	-3.04986573(-3)	2.00068263(-4)	-5.59632427(-4)	-8.62659134(-4)
C_6	-5.10273302(-4)	-5.18423869(-5)	-3.19804466(-4)	-1.25278846(-4)
C_7	-2.72098338(-5)	-5.24546137(-6)	-2.72098338(-5)	-5.24546137(-6)
Mean relative errors				
E(3)	1.827(-2)	2.780(-2)	1.827(-2)	2.780(-2)
E(4)	1.771(-2)	2.613(-2)	1.771(-2)	2.613(-2)
E(5)	1.560(-2)	1.238(-2)	1.560(-2)	1.238(-2)
E(6)	1.443(-2)	9.552(-3)	1.443(-2)	9.552(-3)
E(7)	7.681(-3)	8.329(-3)	7.681(-3)	8.329(-3)

[α] A(b) should read as $A \times 10^b$.

TABLE 3.- ASSUMED H_2O MIXING RATIO AT EQUATOR
(FUNCTION f(z) IN EQ. (12))

Z(km)	f(z)
0	1.09×10^{-2}
1	6.84×10^{-3}
2	4.65×10^{-3}
3	3.42×10^{-3}
4	2.33×10^{-3}
5	1.39×10^{-3}
6	8.55×10^{-4}
7	5.44×10^{-4}
8	3.11×10^{-4}
9	1.55×10^{-4}
10	9.00×10^{-5}
11	5.3×10^{-5}
12	3.05×10^{-5}
13	1.75×10^{-5}
14	1.0×10^{-5}
15	5.8×10^{-6}
16	3.5×10^{-6}

Blank Page

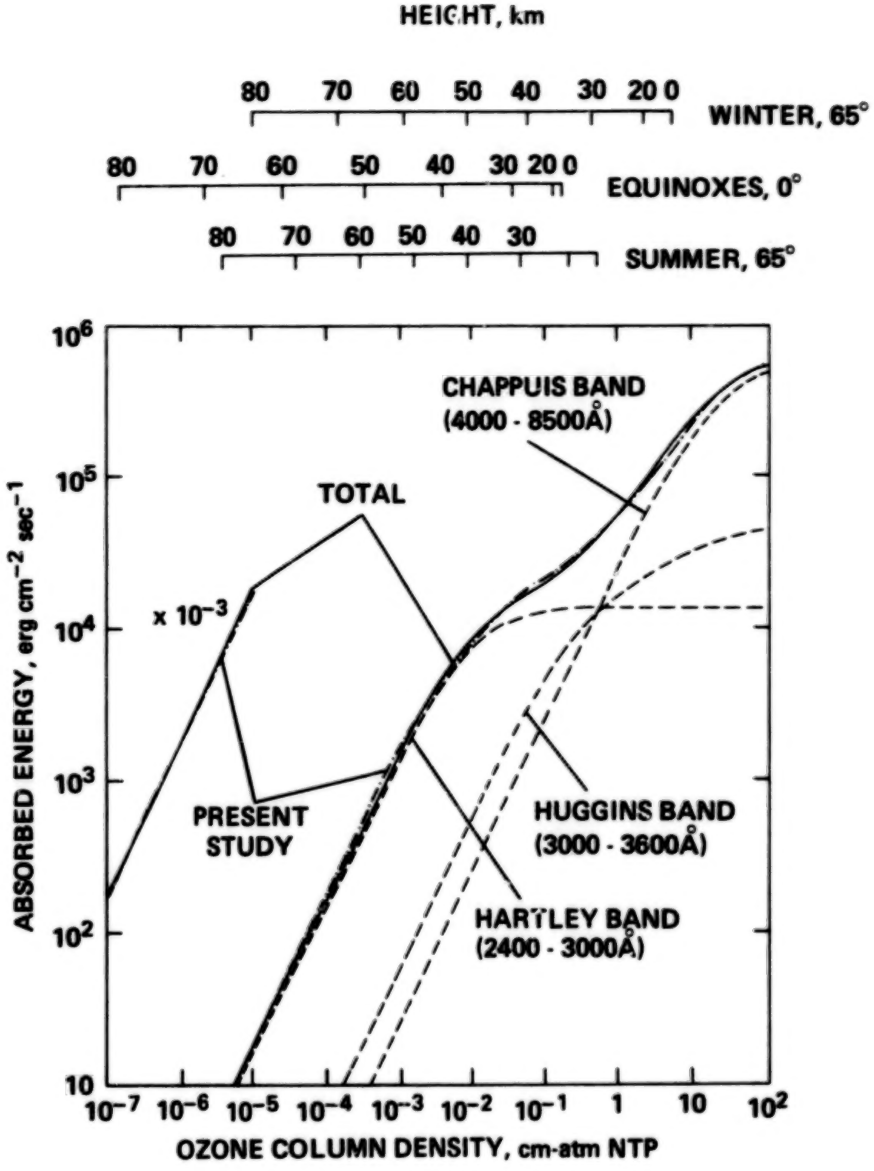

Figure 1.- Absorption by ozone at Hartley band, Huggins band, and Chappuis band. The total of the three bands is compared with the result calculated by our formula. The abscissa indicates the ozone column density, and the corresponding height scales are shown at the top for three representative seasons and latitudes.

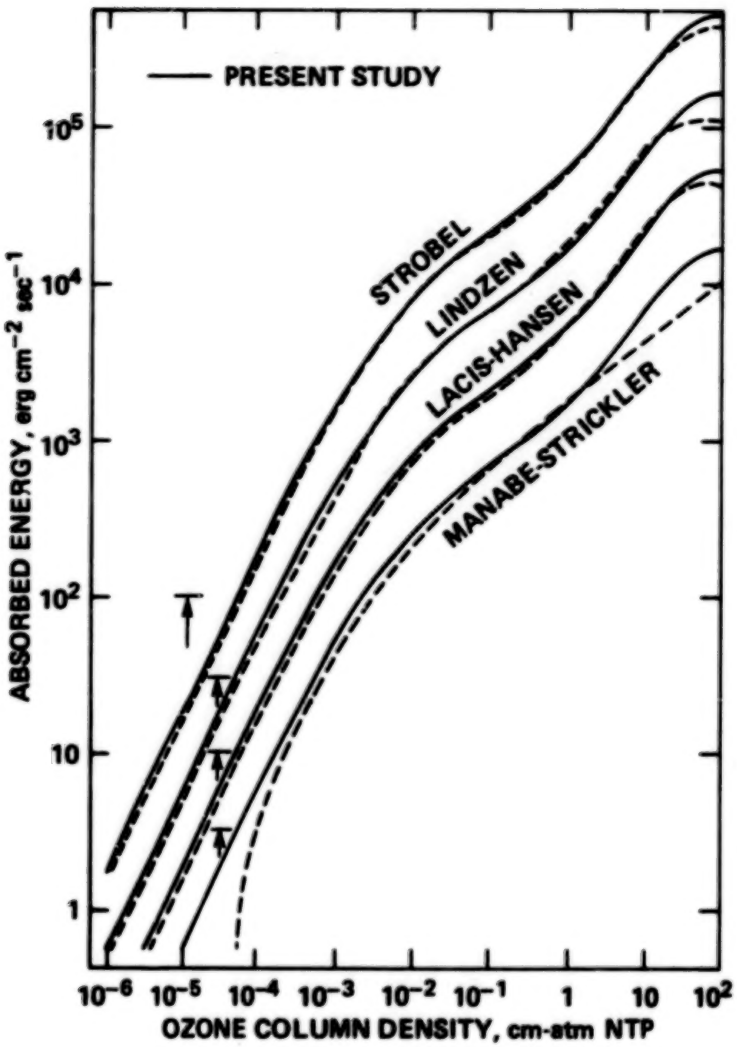

Figure 2.- Comparison of ozone absorption calculated by our formula with those calculated by various other formulae in the literature. Arrows indicate the ordinate at 10^2 erg·cm^{-2} sec^{-1} for each pair of curves.

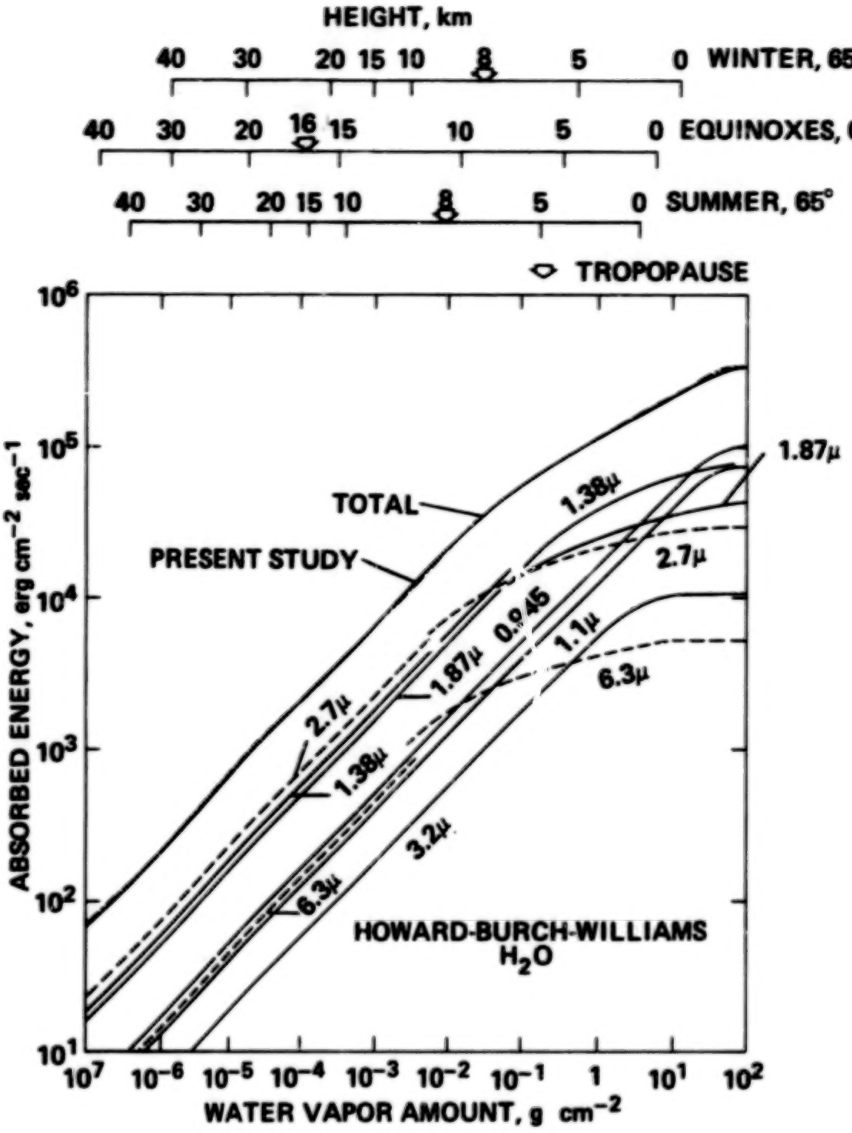

Figure 3.- Absorption by water vapor at seven bands in the range of 0.94 to 6.3 μ calculated by the formulae of Howard et al. (ref. 2). The total of seven bands is compared with the result calculated by our formula.

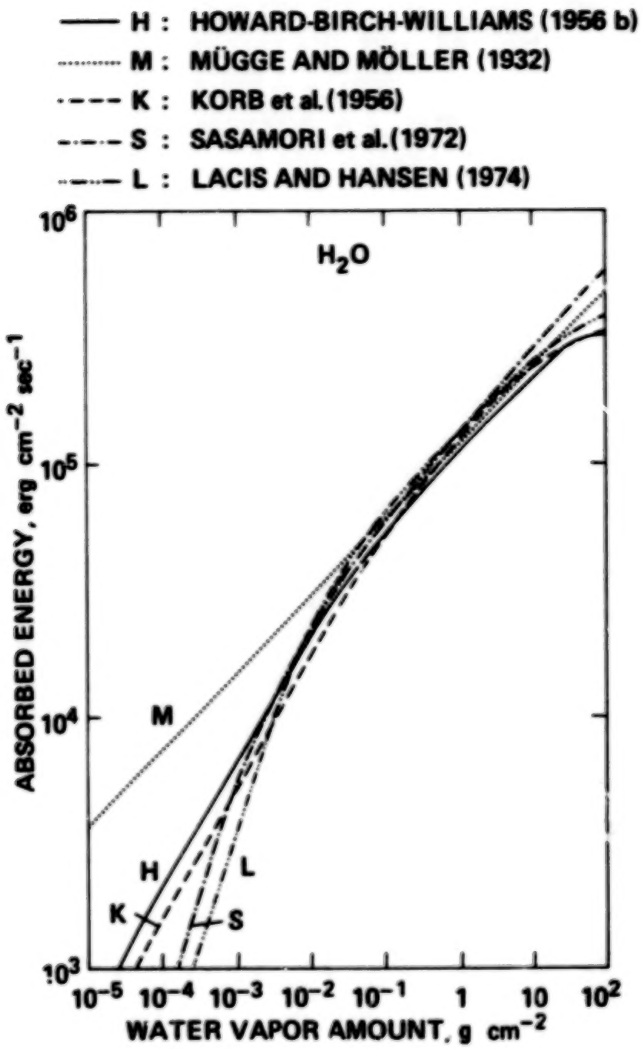

Figure 4.- Comparison of water vapor absorption calculated by various formulae in the literature. Our formula gives the result very close to the curve of Howard et al.

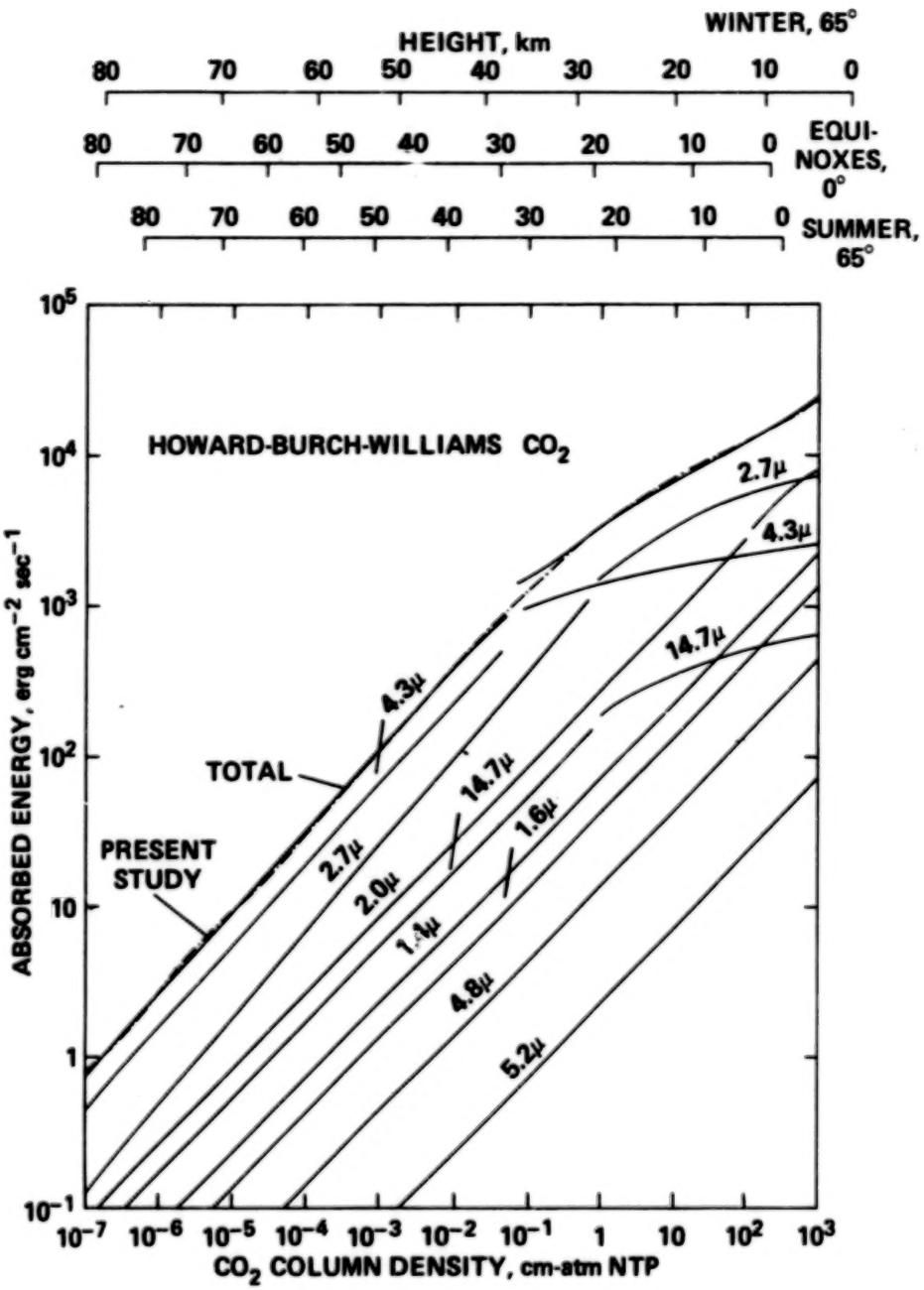

Figure 5.- Absorption by carbon dioxide at eight bands in the range of 1.4 to 14.7 μ calculated by the formulae of Howard et al. (ref. 1). The total of eight bands is compared with the result calculated by our formula. The area of discontinuity at $u \sim 10^{-1}$ cm is smoothed out before the curve-fitting process is applied.

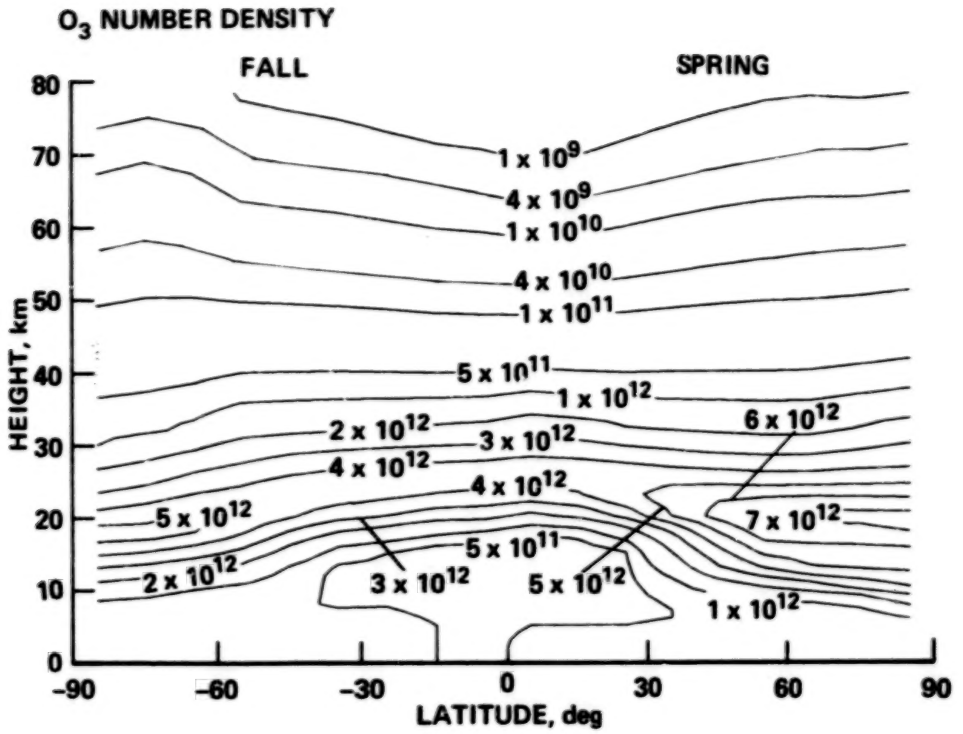

(a) March.

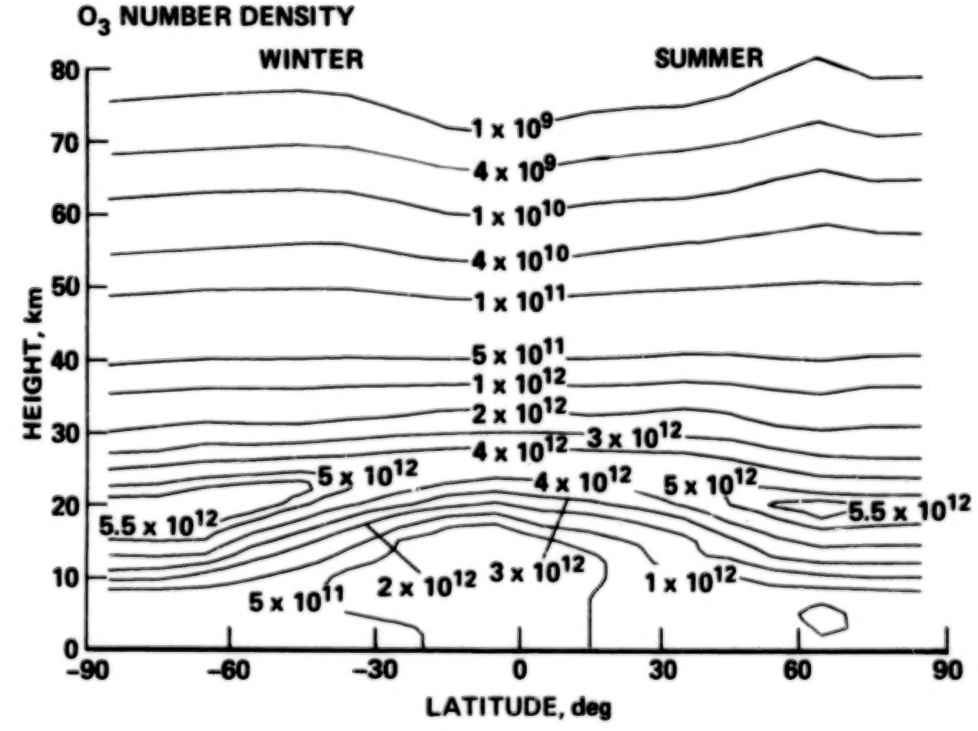

(b) June.

Figure 6.- Latitudinal distribution of the ozone density.

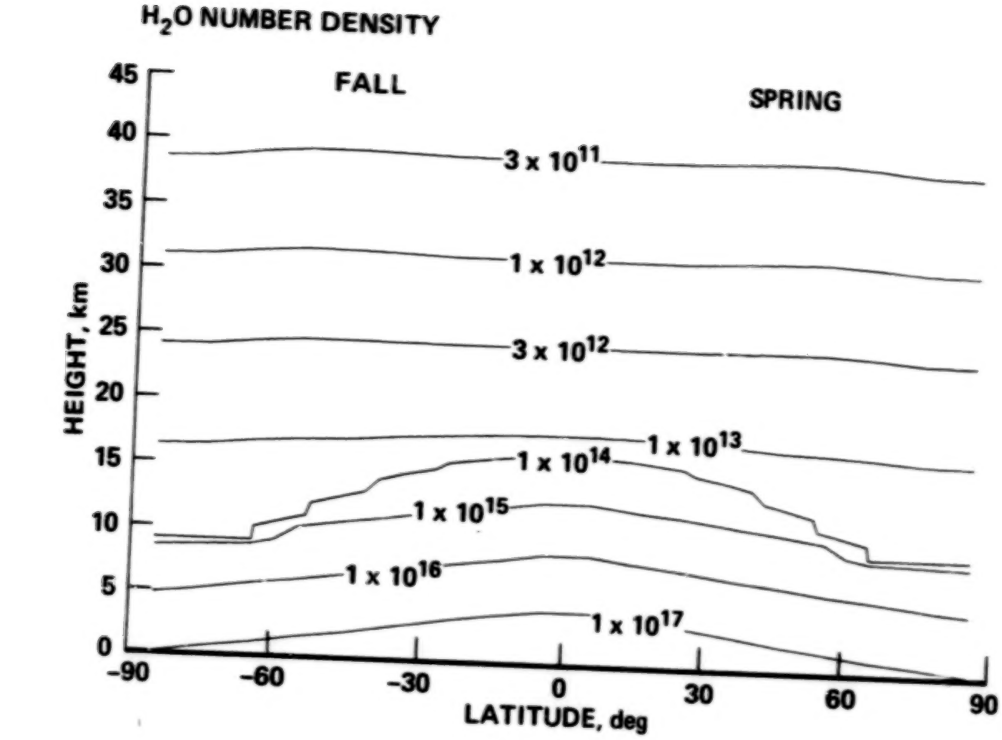

(a) March.

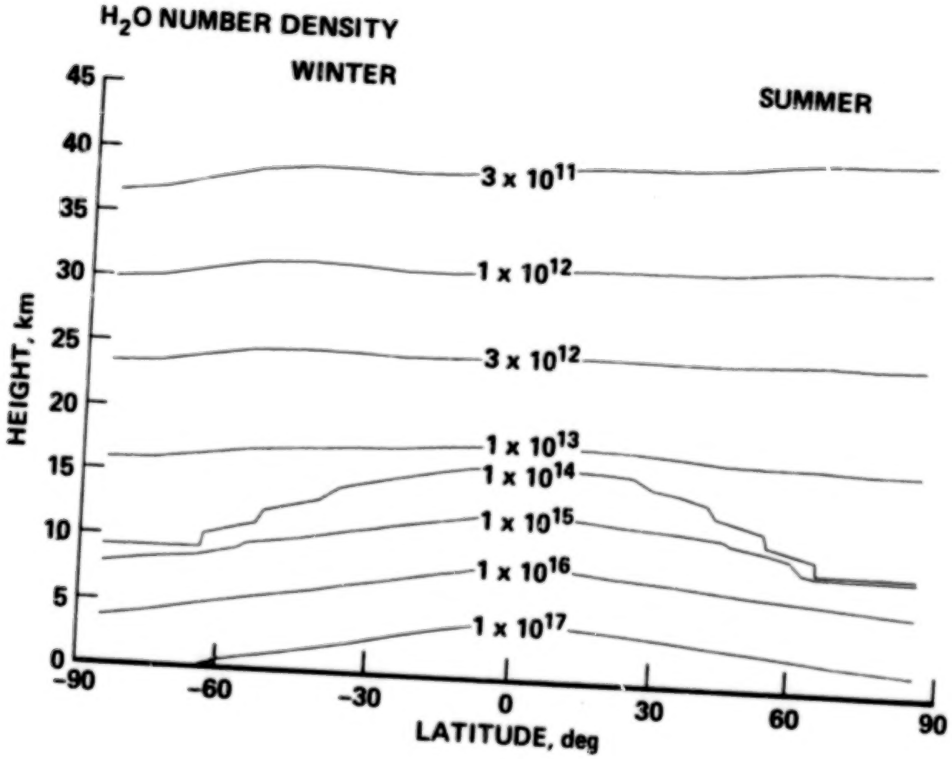

(b) June.

Figure 7.- Latitudinal distribution of the water vapor density.

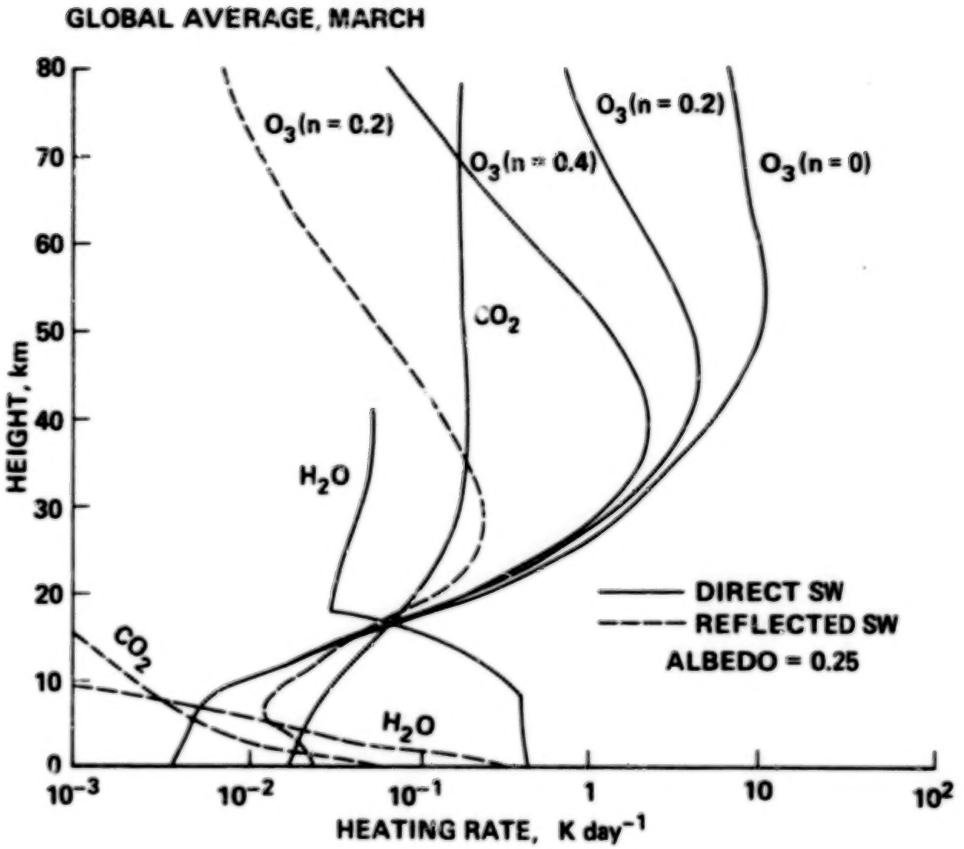

Figure 8.- Height variation of the heating rate due to O_3, H_2O and CO_2 absorption, representing the global average for March. The heating rate due to reflected waves is calculated assuming an effective albedo of 0.25. A very large pressure effect appears on the ozone heating above ~40 km. The value of n = 0.2 was adopted in the present study.

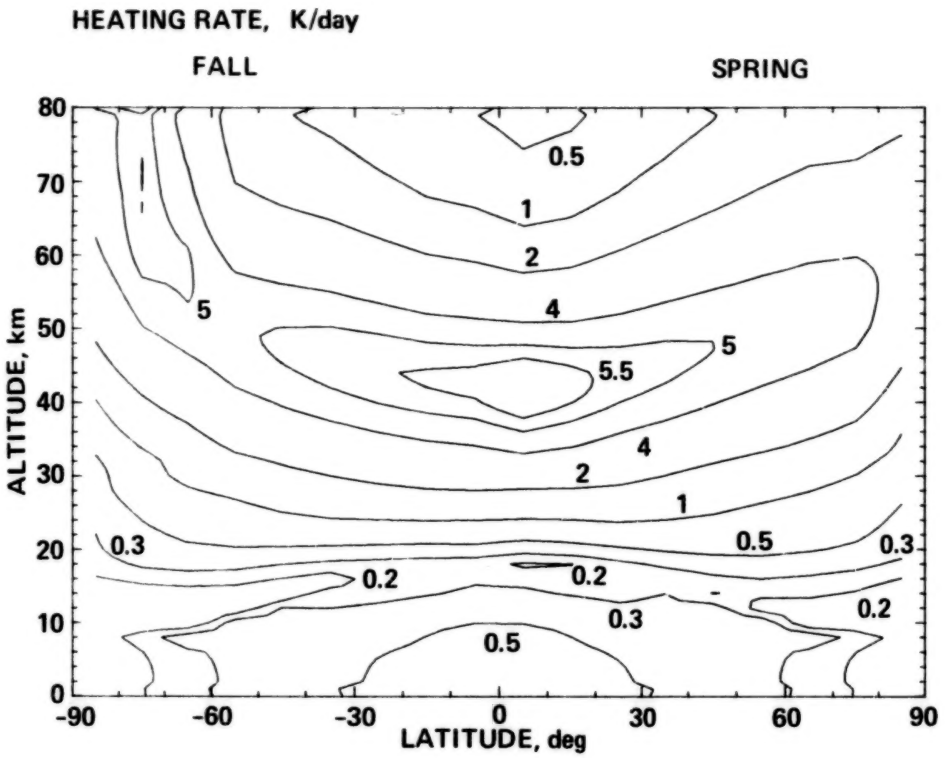

(a) March.

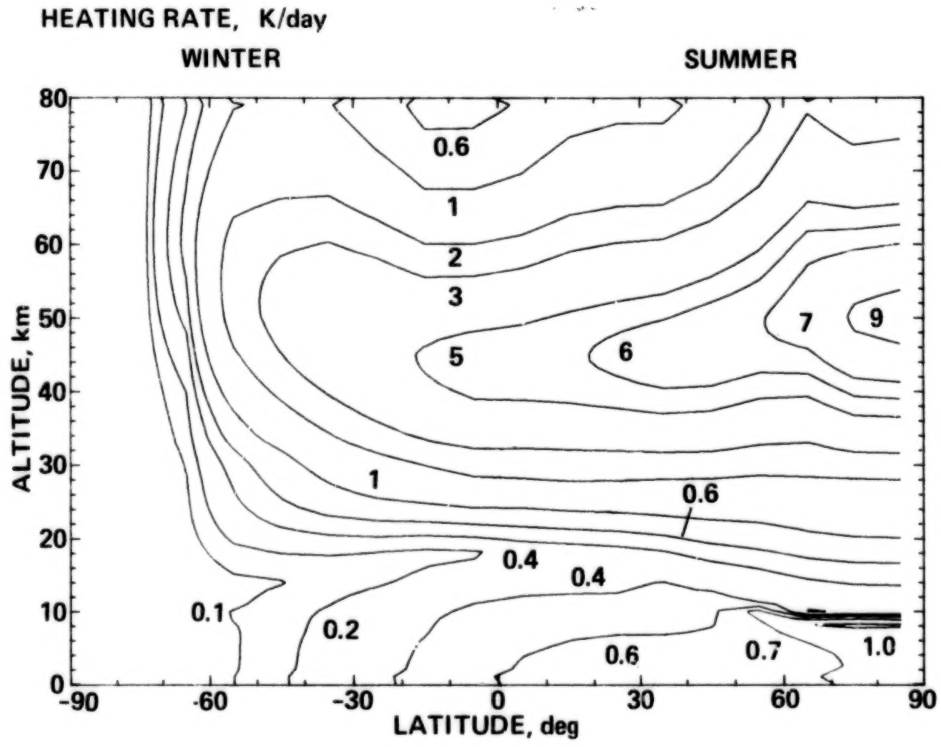

(b) June.

Figure 9.- Latitudinal distributions of the diurnal heating rate.

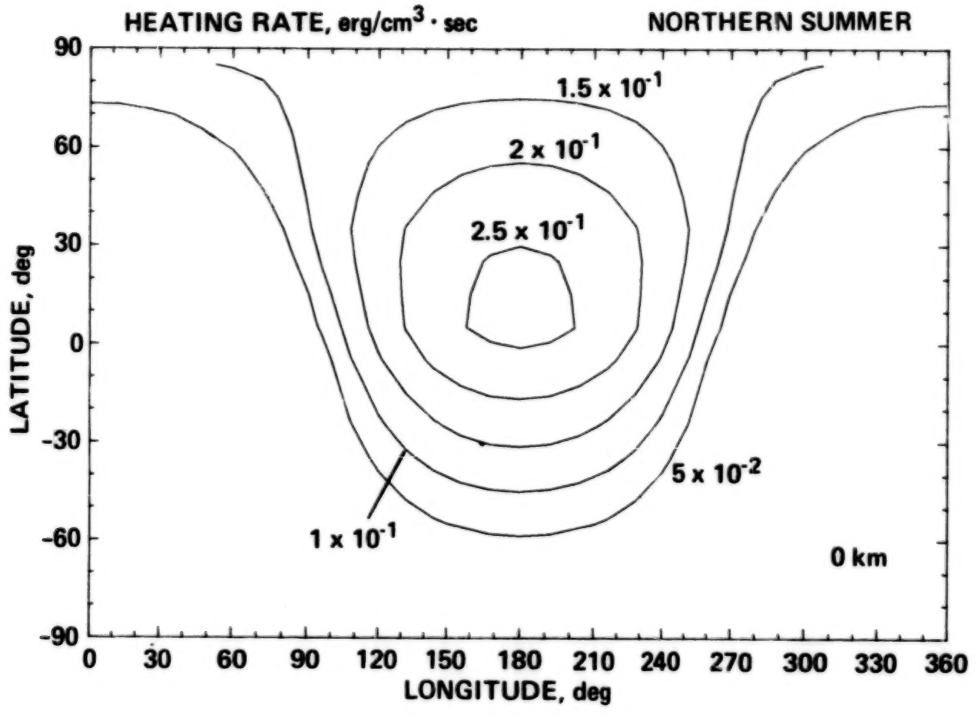

(a) 0 km

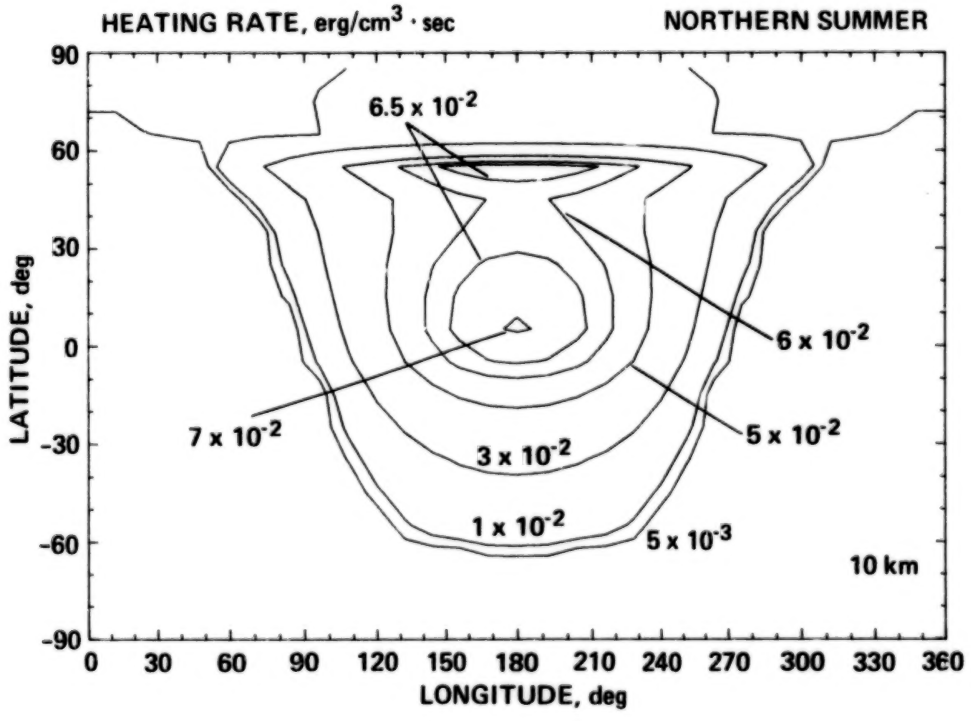

(b) 10 km

Figure 10.- Horizontal distributions of the heating rate for June.

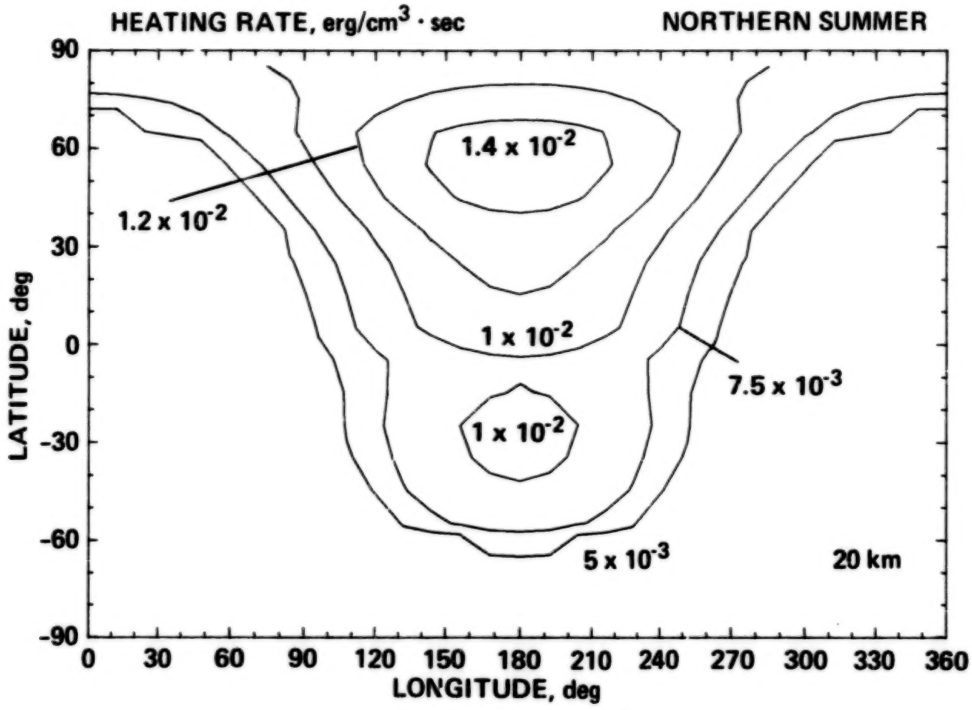

(c) 20 km

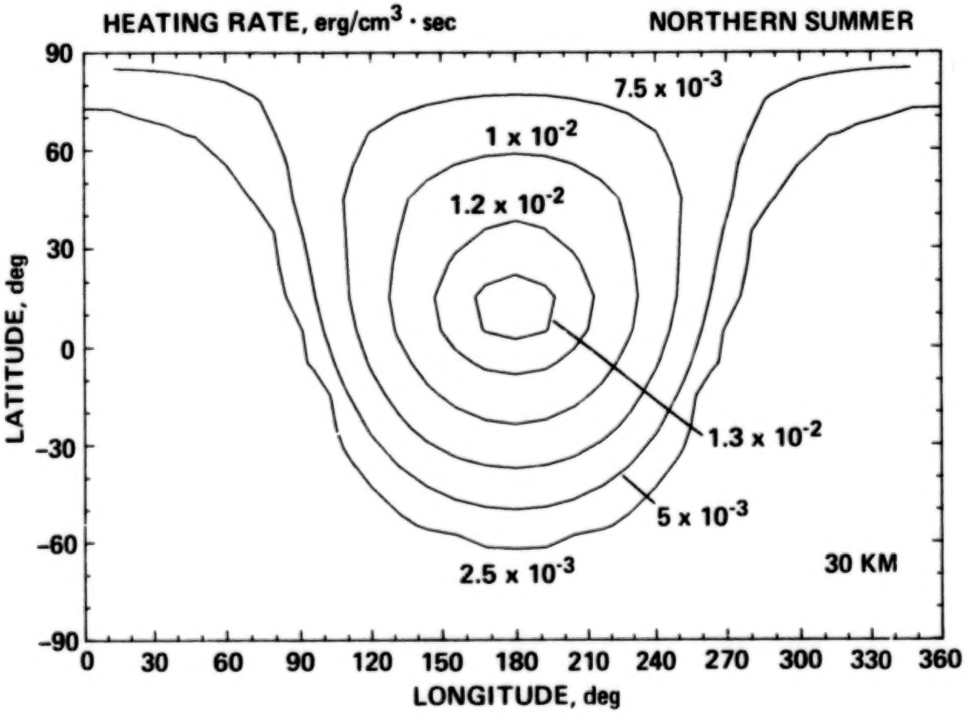

(d) 30 km

Figure 10.- Continued.

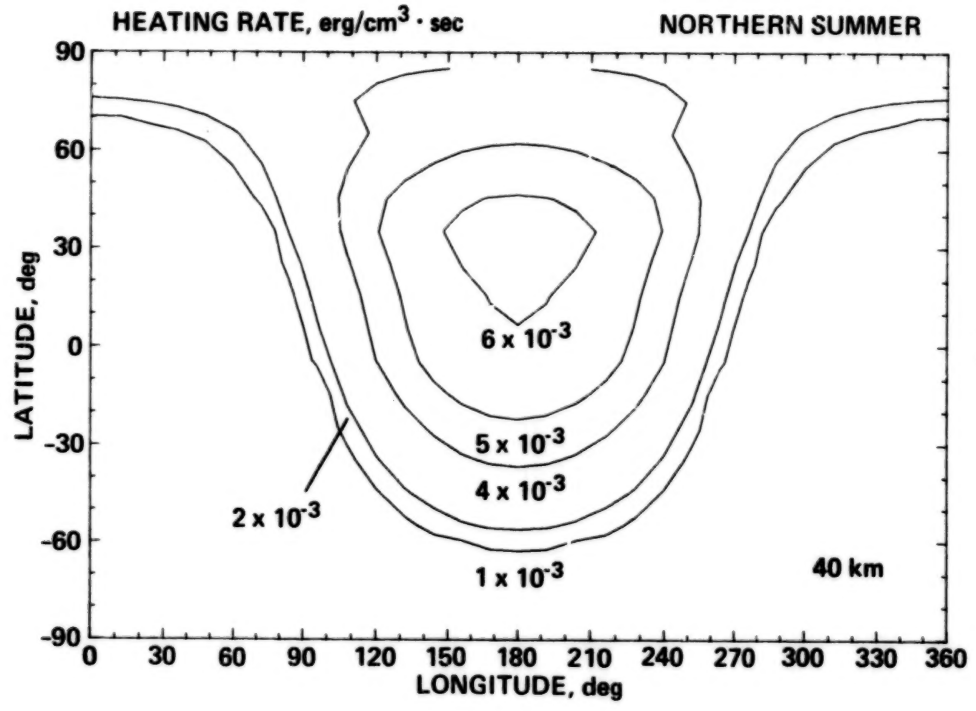

(e) 40 km

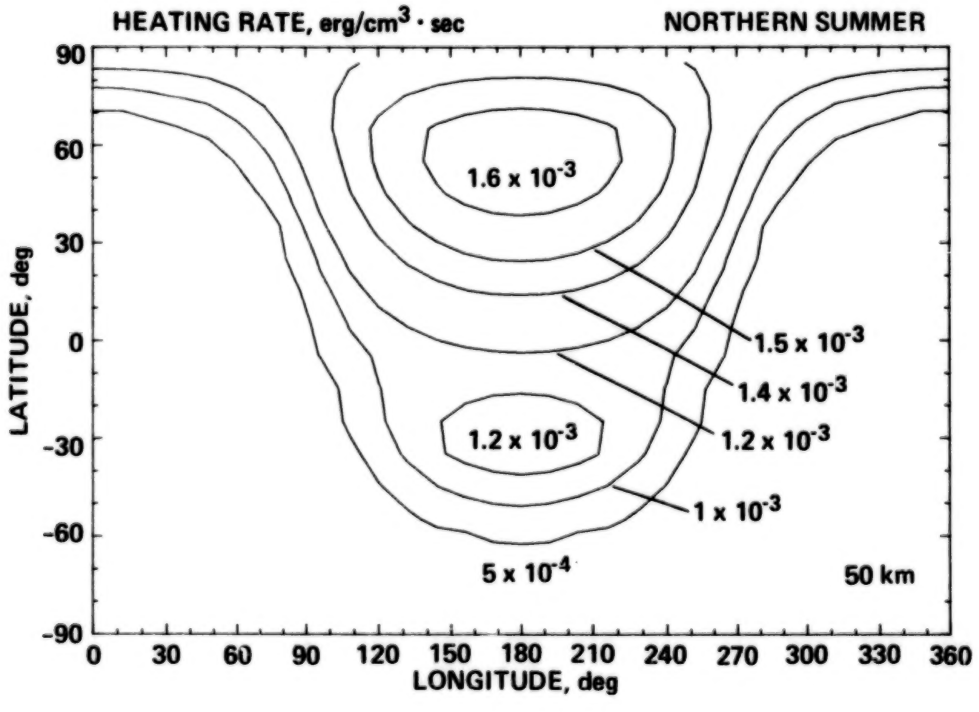

(f) 50 km

Figure 10.- Continued.

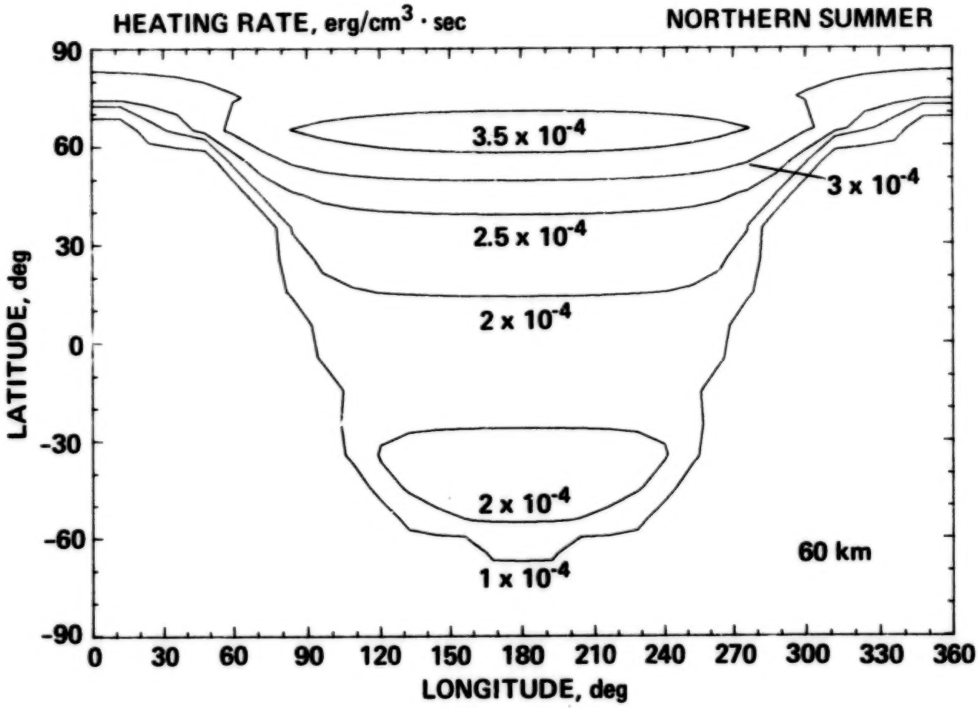

(g) 60 km

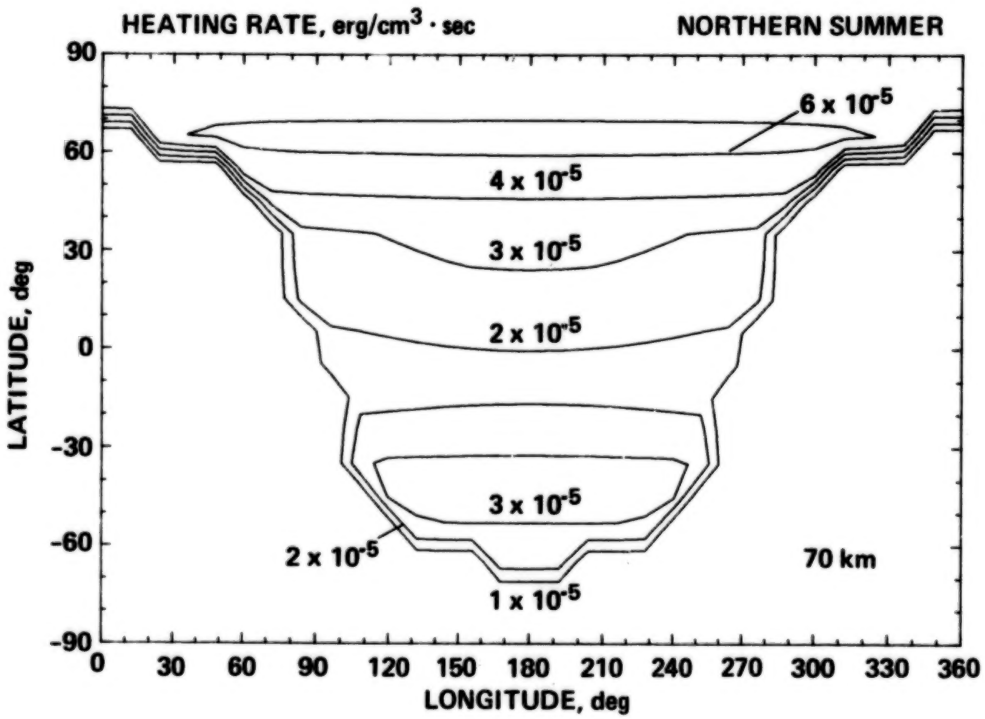

(h) 70 km

Figure 10.- Concluded.

1. Report No.	2. Government Accession No.	3. Recipient's Catalog No.
NASA TP-1398		

4. Title and Subtitle	5. Report Date
A SIMPLIFIED METHOD FOR CALCULATING THE ATMOSPHERIC HEATING RATE BY ABSORPTION OF SOLAR RADIATION IN THE STRATOSPHERE AND MESOSPHERE	January 1979
	6. Performing Organization Code

7. Author(s)	8. Performing Organization Report No.
Tatsuo Shimazaki and Leland C. Helmle*	A-7557
	10. Work Unit No.
	198-30-02

9. Performing Organization Name and Address	11. Contract or Grant No.
Ames Research Center, NASA Moffett Field, Calif. 94035	
	13. Type of Report and Period Covered
12. Sponsoring Agency Name and Address	Technical Paper
National Aeronautics and Space Administration Washington, D. C., 20546	14. Sponsoring Agency Code

15. Supplementary Notes

*Informatics, Inc., Palo Alto, California 94303

16. Abstract

A simple analytical formula is worked out for calculations of the atmospheric heating rate by absorption of solar radiation by O_3, H_2O, and CO_2. The method needs only seven parameters for each molecule and can save computational time and memory locations. It is particularly useful for heating calculations in three-dimensional global circulation models below 80 km. Applying the formula to the observed distributions of O_3, H_2O, and CO_2 produces reasonable latitudinal and seasonal variations in the heating rate. The calculated heating rate, however, is sensitive to the global distributions of the absorbing gases, and uncertainties in the O_3 distribution above ~50 km and the H_2O distribution below ~20 km may seriously affect the global distributions of the heating rate in these regions.

17. Key Words (Suggested by Author(s))	18. Distribution Statement
Atmospheric heating Absorption of solar radiation	Unlimited STAR Category - 47

19. Security Classif. (of this report)	20. Security Classif. (of this page)	21. No. of Pages	22. Price*
Unclassified	Unclassified	32	$4.00

*For sale by the National Technical Information Service, Springfield, Virginia 22161

NASA-Langley, 1979

END

APR 30 1979